



ELSEVIER

Novel iron(III) complexes with imidazole containing tripodal ligands as model systems for catechol dioxygenases[☆]

Matthias Pascaly^a, Mark Duda^a, Annette Rompel^a, Bernd H. Sift^a,
Wolfram Meyer-Klaucke^b, Bernt Krebs^{a,*}

^a Anorganisch-Chemisches Institut der Westfälischen Wilhelms-Universität, Wilhelm-Klemm-Str. 8, D-48149 Münster, Germany

^b EMBL Outstation Hamburg c/o DESY, Notkestr. 85, D-22603 Hamburg, Germany

Received 27 November 1998; accepted 1 March 1999

Abstract

The iron(III) complexes [Fe(bpia)Cl₂][FeCl₄] (**1**), [Fe(bipa)Cl₂](ClO₄) (**2**), and [Fe₂O(bpia)₂Cl₂]Cl₂(4MeOH) (**3**) (bpia: bis[(2-pyridyl)methyl][(1-methylimidazol-2-yl)methyl]amine, bipa: bis[(1-methylimidazol-2-yl)methyl][(2-pyridyl)methyl]amine) were synthesized. **1** and **2** are structural and functional models for catechol 1,2-dioxygenase. All compounds are characterized by spectroscopic methods and X-ray structure analysis. **3** was also investigated by EXAFS. The coordination environment around all Fe(III) cores is distorted octahedral by the tripodal ligand, chloride, and in the case of **3**, additionally, oxygen. Chloride and oxygen are bonded labile in the functionally essential *cis* positions to the iron core. These are the binding sites of the catechol. The cation in **3** is formed as a dimerization product of **1** so that the oxo ligand acts as a linear bridge with a Fe...Fe separation of 3.5756(8) Å. These properties of **3** have been used to study the amplitude enhancement in the EXAFS signal due to multiple scattering. In situ prepared iron(III) complexes with the ligands bpia and bipa show significant intradiol catechol dioxygenase activity with respect to the cleavage of 3,5-di-tert-butylcatechol and pyrocatechol. © 1999 Elsevier Science S.A. All rights reserved.

Keywords: Iron complexes; Tripodal ligand complexes; Crystal structures; Catechol dioxygenase model complexes; X-ray absorption spectroscopy

1. Introduction

Non-heme iron proteins with mono- and dinuclear active sites have attracted considerable attention. Mononuclear enzymes are involved in processes including the biosynthesis of isopenicillin N (isopenicillin N synthases) [1], oxidation of unsaturated fatty acids (lipoxygenases) [2] and oxidative cleavage of aromatic diols (catechol dioxygenases) [3]. The important class of catechol dioxygenases takes part in nature's mechanism for metabolizing aromatic substrates to aliphatic products by insertion of both atoms of O₂ into the substrate. These metalloproteins are subdivided into intradiol and

extradiol enzymes according to their catalysis of aromatic ring cleavage between or outside the two *ortho*-hydroxo groups. Intradiol dioxygenases contain iron(III), whereas extradiol dioxygenases contain iron(II) in their active sites.

Complexes with various ligands have been used for modeling the properties of catechol 1,2-dioxygenases [4–6]. Especially tetradentate tripodal ligands have proven to be able to regulate the dioxygenase reactivity of biomimetic iron model complexes [7–12]. Tripodal ligands form distorted complexes with two unoccupied *cis* coordination sites for binding catecholate. The heterocyclic organic compounds bpia (bis[(2-pyridyl)methyl][(1-methylimidazol-2-yl)methyl]amine) and bipa (bis[(1-methylimidazol-2-yl)methyl][(2-pyridyl)methyl]amine) belong to the class of tripodal ligands that provide N₄ donor sets. These are the first tripodal ligands with methylimidazole moieties used for modeling catechol 1,2-dioxygenases. The methylimidazole moieties are closely related to the amino acid histidine which coordinates the metal cores in enzymes. There-

[☆] Dedicated to Professor Heinz Dieter Lutz on the occasion of his 65th birthday.

* Corresponding author. Tel.: +49-251-83 331 31; fax: +49-251-83 383 66.

E-mail address: krebs@nwz.uni-muenster.de (B. Krebs)

fore, the ligands model the coordinative aspects in metalloenzymes better than ligands synthesized before.

Usually 3,5-di-tert-butylcatechol (dbc) has been used as the substrate in functional investigations. The observed cleavage product is quite stable and has been identified as 3,5-di-tert-butyl-1-oxacyclohepta-3,5-dien-2,7-dione (anhydride of the *cis,cis*-muconic acid), the immediate product of oxygen insertion into dbc (Fig. 1) [8,9,13]. In previous studies Duda et al. have examined the oxygenation reactivity of catechols depending on their substituents [14].

In this paper we report the synthesis, structural, and spectroscopic characterization of a series of novel iron(III) compounds as functional and structural model complexes for catechol 1,2-dioxygenases: $[\text{Fe}(\text{bpia})\text{Cl}_2][\text{FeCl}_4]$ (**1**) and $[\text{Fe}(\text{bipa})\text{Cl}_2](\text{ClO}_4)$ (**2**) providing two *cis* coordination sites for substrate binding which are occupied with labile chloro ligands. For comparison we also report the structure of the μ -oxo bridged dimer $[\text{Fe}_2\text{O}(\text{bpia})_2\text{Cl}_2]\text{Cl}_2 \cdot 4\text{MeOH}$ (**3**) in which one chloro ligand is replaced by the labile μ -oxo bridge. This dinuclear species is postulated to be formed at the end of the reaction of the mononuclear bpia iron complex with catechol and O_2 [14]. In analogy to previous investigations it can be assumed that the complexes transform into the reactive species by substitution of the chloro ligands (for **1** and **2**) and by the cleavage of the oxo bridge (for **3**) so that these compounds function as precursor complexes for reactive species in solution [15].

The oxo complex **3** presents a significant challenge for multiple scattering (MS) EXAFS analysis (extended X-ray absorption fine structure). MS effects are expected to become especially significant for a monoatomic bridge which approaches linearity [16,17]. Since there are not many complexes with a linear monoatomic oxo bridge we performed EXAFS analysis on compound **3** to study the significant amplitude enhancement in the EXAFS signal.

For the investigation of catechol-cleaving activity of in situ prepared mononuclear complexes UV–Vis spectroscopic studies were carried out with dbc and pyrocatechol (cat) as substrates to study the influence of the ligand and the catechol on the reaction rate.

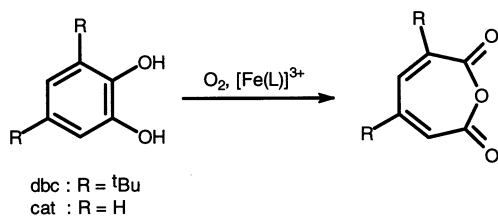


Fig. 1. Oxidative cleavage of catechols.

2. Experimental

2.1. Materials

All chemicals were of reagent grade and used as received.

2.2. Physical measurements

IR spectra were obtained as KBr pellets on a Bruker IFS 48 spectrometer in the range of 4000–400 cm^{-1} . ^1H and ^{13}C NMR spectra were measured on a Bruker WH300 spectrometer. The electronic absorption spectra were recorded on a Kontron spectrophotometer UVIKON 933 using quartz cuvettes (1 cm) and methanol as solvent ($c = 2.5 \times 10^{-4} \text{ mol l}^{-1}$). Time dependent UV–Vis spectroscopy was performed on a Hewlett Packard Diode Array spectrometer. Elemental analyses were carried out at the Organisch-Chemisches Institut der Universität Münster on a Heraeus CHN-O-Rapid analyzer. Cyclic voltammograms were measured on a BAS CV-50W electrochemical analyzer under Ar atmosphere using a graphite working electrode with 0.1 M tetrabutylammonium tetrafluoroborate as supporting electrolyte and $10^{-4} \text{ mol l}^{-1}$ of the analyt at 25°C. Voltages are recorded relative to Ag/AgCl. The Mössbauer spectrum was measured in transmission at 293 K at the Physikalisch-Chemisches Institut der Universität Münster using a 28 mCi source of ^{57}Co in Co metal. Velocity calibration was carried out by the resonance lines of α -iron, and the isomer shift was given relative to α -iron at room temperature. Magnetic susceptibility of a powdered sample was recorded on a Faraday-type magnetometer using a Cahn RG electrobalance in the temperature range 4.5–320 K. The applied magnetic field was about 1.5 T. Details of the apparatus have been described elsewhere [18]. The experimental susceptibility data were collected for the underlying diamagnetism in the usual manner using Pascal's constants [19]. Correction for diamagnetism was estimated as $-546.6 \times 10^{-6} \text{ cm}^3 \text{ mol}^{-1}$. From the magnetic susceptibility the effective magnetic moment μ_{eff} was derived following $\mu_{\text{eff}}[\mu_{\text{B}}] = \sqrt{8\chi T}$.

2.3. X-ray absorption spectroscopy

2.3.1. EXAFS measurements

The sample of **3** was enclosed in an appropriate cell with kapton foil windows and measured at beamline E4 (DORIS III storage ring at HASYLAB) with an electron beam energy of 4.5 GeV and an average current of 80 mA. Fe K-edge XAS experiments resembled those previously described for Fe [20] and Cu [21] model complexes measured in absorption mode. For energy calibration, the spectrum of α -iron was measured simultaneously, the first inflection point of which was as-

signed to the value 7112.0 eV. Reproducibility of the Fe K-edge energies in the above conditions has been found previously to be ± 0.1 eV [20]. Spectra were collected from 6800 to 8120 eV. Four scans were recorded and the average analyzed.

2.3.2. Data analysis

To analyze Fe EXAFS data, we followed a procedure similar to the one used for other Fe [20] and Cu [21] model compounds. The k -space data were truncated near the zero crossing ($k = 3.5\text{--}16 \text{ \AA}^{-1}$) before the Fourier transform was applied. Raw data were analyzed. The back-transformed, Fourier isolated data in k -space were then subjected to curve fitting using the full curved wave approach from the program EXCURV92 [22].

The wide-shell filtered data were fitted using constrained refinement of the imidazole groups including their multiple scattering contributions as described in Ref. [23]. The imidazole rings are treated as a geometrically rigid unit.

A value of 0.7 was used for the amplitude reduction factor and a value of -1.0 eV for the constant imaginary potential which describes the lifetime of the photoelectrons and the value E_0 is refined for all shells together.

The quality of the fit is represented by the R -factor which is given as

$$R = \frac{\sum_{i=1}^N \frac{k_i^n}{\sum_{j=1}^N k_j^n} |\chi_i^{\text{exp}}(k_i) - \chi_i^{\text{th}}(k_i)|}{\sum_{j=1}^N k_j^n |\chi_j^{\text{exp}}(k_j)|} \times 100\%$$

where $\chi^{\text{exp}}(k)$ and $\chi^{\text{th}}(k)$ are the experimental and theoretical EXAFS [22].

The maximum number of parameters allowed to vary simultaneously in the curve-fitting analysis was estimated by $N_{\text{free}} = 2\Delta R_{\text{FF}}\Delta k_{\text{fit}}/\pi$ where ΔR_{FF} is the width of the filter window and Δk_{fit} is the length of the data set in k space.

2.4. Synthesis of the ligands bis[(2-pyridyl)methyl]-[(1-methylimidazol-2-yl)methyl]amine (bpia) and bis[(1-methylimidazol-2-yl)methyl][(2-pyridyl)methyl]amine (bipa)

The ligands (Fig. 2) were prepared according to a procedure described in the literature [24]. Modifications were made in the syntheses of the preliminary products (1-methylimidazol-2-yl)methanol and bis((2-pyridyl)methyl)amine to improve the conversion to the product.

2.4.1. (1-Methylimidazol-2-yl)methanol

The followed procedure was first described by Reese and Pei-Zhou [25]. A mixture of 30.0 g (0.365 mol) 1-methylimidazole and 30.0 g (1 mol) paraformalde-

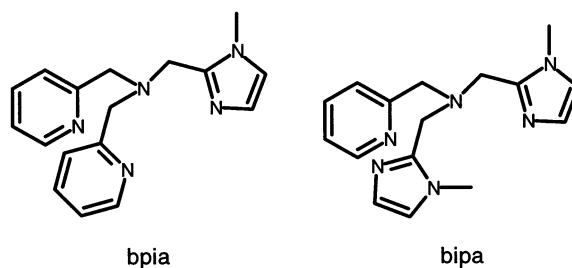


Fig. 2. The tripodal ligands bpia and bipa used in this work.

hyde was heated at 160°C for 2 h. After cooling to room temperature the mixture was solved in methanol. The product precipitated as a light brown powder at -20°C . This crude product was recrystallized from CHCl_3 to yield yellow crystals (16.2 g, 0.144 mol, 39%); m.p. 114°C . ^1H NMR (CDCl_3) δ (ppm): 3.6 (s, 3H), 4.4 (s, 2H), 4.7–5.3 (m, 1H), 5.8 (d, 1H), 6.5 (d, 1H).

2.4.2. Bis((2-pyridyl)methyl)amine

A total of 15.0 g (0.139 mol) of ((2-pyridyl)methyl)amine and 15.0 g (0.140 mol) of pyridine-2-carboxaldehyde were stirred together in 60 ml methanol. After 2 h 1.9 g (0.054 mol) NaBH_4 were added at 0°C . The resulting red solution was stirred overnight and additionally refluxed for 1 h. The solution was allowed to cool to room temperature diluted with 10 ml water and acidified (pH 1) with hydrochloric acid to yield the amine as a hydrochloride. To separate impurities and side products this mixture was extracted with CHCl_3 (5×20 ml). In order to neutralize the hydrochloride the pH was adjusted to 8 with an aqueous solution of NaOH . The free amine was extracted with CHCl_3 (4×20 ml). The combined organic layers were dried (MgSO_4) and concentrated under reduced pressure. High vacuum distillation yielded 17.6 g (0.089 mol, 64%) of the product; b.p. $145\text{--}150^\circ\text{C}$ (1 mmHg). ^1H NMR (CDCl_3) δ (ppm): 2.6 (s, 1H), 4.0 (s, 4H), 7.13 (t, 2H), 7.37 (d, 2H), 7.63 (t, 2H), 8.58 (d, 2H). ^{13}C NMR (CDCl_3) δ (ppm): 54.79 (CH_2), 121.92 (C_{ar}), 122.27 (C_{ar}), 136.41 (C_{ar}), 149.31 (C_{ar}), 159.73 (C_{ar}).

CAUTION: Perchlorate salts of metal complexes with organic ligands are potentially explosive.

2.5. Synthesis of $[\text{Fe}(\text{bpia})\text{Cl}_2][\text{FeCl}_4]$ (1)

To a solution of 50 mg (0.18 mmol) bpia in 5 ml methanol a solution of 29 mg (0.18 mmol) FeCl_3 in 1 ml methanol was added and refluxed together for 5 min. After vapor diffusion of ether into the hot solution red crystals suitable for X-ray diffraction analysis were deposited after a few days. Yield: 45 mg (0.074 mmol, 41%); m.p. 153°C . Anal. Calc. for $\text{C}_{17}\text{H}_{19}\text{N}_5\text{Cl}_6\text{Fe}_2$: C, 33.1; H, 3.1; N, 11.3. Found: C, 33.9; H, 3.9; N, 10.9%.

2.6. Synthesis of $[\text{Fe}(\text{bipa})\text{Cl}_2](\text{ClO}_4)$ (**2**)

A total amount of 9 mg (0.017 mmol) of $\text{Fe}(\text{ClO}_4)_3 \cdot 9\text{H}_2\text{O}$ and 9 mg (0.035 mmol) of FeCl_3 were solved together in 5 ml of a methanol + ethanol mixture (4:3). After addition of 15 mg (0.052 mmol) bipa in 15 ml of the same solvent the solution was heated until reflux. Upon standing for 24 h red crystals suitable for X-ray diffraction were obtained. Yield: 15 mg (0.028 mmol, 53%); decomposition over 210°C. Anal. Calc. for $\text{C}_{16}\text{H}_{20}\text{N}_6\text{Cl}_3\text{FeO}_4$: C, 36.8; H, 3.9; N, 16.1. Found: C, 36.7; H, 3.7; N, 15.8%.

2.7. Synthesis of $[\text{Fe}_2\text{O}(\text{bipa})_2\text{Cl}_2]\text{Cl}_2 \cdot 4\text{MeOH}$ (**3**)

To a solution of 74 mg (0.3 mmol) bipa and 8.8 μl (0.0064 mg, 0.063×10^{-6} mol) triethylamine in 5 ml methanol a solution of 82 mg (0.3 mmol) $\text{FeCl}_3 \cdot 9\text{H}_2\text{O}$ in 1 ml methanol was added. After vapor diffusion of diethyl ether into this solution 43 mg (0.044 mmol, 29%) black crystals precipitated suitable for X-ray analysis; m.p. 144°C. Anal. Calc. for $\text{C}_{38}\text{H}_{50}\text{N}_{10}\text{Cl}_4\text{Fe}_2\text{O}_5$: C, 46.5; H, 5.1; N, 14.3. Found: C, 44.5; H, 5.5; N, 14.7%.

2.8. Crystallography

The unit-cell data and diffraction intensities of compounds **1** and **3** were collected on a STOE imaging-plate diffraction system at 213 K using Mo $\text{K}\alpha$ radiation (graphite monochromated, $\lambda = 0.71073 \text{ \AA}$). The sample-to-plate distance was fixed at 70 mm for **1** (60 mm for **3**) with a scan range from $0 \leq \theta \leq 300^\circ$ for **1** ($0 \leq \theta \leq 180^\circ$ for **3**) with an exposure time of 2 min and an oscillating angle of $\Delta\theta = 3^\circ$ for **1** and $\Delta\theta = 2^\circ$ for **3**, respectively. Intensity data for complex **2** were collected on an Enraf–Nonius CAD4 (Mo $\text{K}\alpha$, 0.71073 \AA , graphite monochromator), by using the ω -scan technique with a variable scan rate of 2.93–29.30° min^{-1} . Further crystal data and experimental parameters are listed in Table 1.

The structures of **1** and **3** were solved by direct methods, structure **2** was solved by a Patterson synthesis using the program system SHELXS 86. All other non-hydrogen atoms were taken from a series of full-matrix least-squares refinement cycles based on F^2 with the SHELXL 93 program followed by difference Fourier syntheses [26].

Table 1
Crystallographic data and experimental details

	$[\text{Fe}(\text{bipa})\text{Cl}_2][\text{FeCl}_4]$ (1)	$[\text{Fe}(\text{bipa})\text{Cl}_2](\text{ClO}_4)$ (2)	$[\text{Fe}_2\text{O}(\text{bipa})_2\text{Cl}_2]\text{Cl}_2 \cdot 4\text{MeOH}$ (3)
Formula	$\text{C}_{17}\text{H}_{19}\text{N}_5\text{Fe}_2\text{Cl}_6$	$\text{C}_{16}\text{H}_{20}\text{N}_5\text{Cl}_3\text{FeO}_4$	$\text{C}_{38}\text{H}_{50}\text{N}_{10}\text{Cl}_4\text{Fe}_2\text{O}_5$
M (g mol^{-1})	617.77	522.58	980.39
Crystal system	monoclinic	monoclinic	triclinic
Space group	$P2_1$ (No. 4)	$P2_1/n$ (No. 14)	$P\bar{1}$ (No. 2)
a (\AA)	9.538(2)	9.110(2)	9.244(2)
b (\AA)	11.699(2)	15.450(3)	11.002(2)
c (\AA)	11.225(2)	15.869(3)	12.507(3)
α ($^\circ$)	90	90	68.74(3)
β ($^\circ$)	101.57(3)	106.18(3)	77.62(3)
γ ($^\circ$)	90	90	83.40(3)
V (\AA^3)	1227.1(4)	2145.1(4)	1156.9(4)
Formula units/uc	2	4	1
ρ_c (g cm^{-3})	1.672	1.618	1.407
T (K)	213(2)	298(2)	213(2)
Absorption coefficient (mm^{-1})	1.850	1.113	0.771
$F(000)$	620	1068	376
Data collection range ($^\circ$)	$8.7 \leq 2\theta \leq 52.2$	$3.8 \leq 2\theta \leq 51.9$	$10.8 \leq 2\theta \leq 52.0$
Reflections measured	14478	4476	8085
Independent reflections	4724 ($R_{\text{int}} = 0.0571$)	4204 ($R_{\text{int}} = 0.0241$)	4191 ($R_{\text{int}} = 0.0403$)
Reflections observed ($I > 2\sigma(I)$)	4539	3577	3808
Variables	271	271	271
Goodness-of-fit (F_o^2)	1.084	1.039	1.009
Final R value ($I > 2\sigma(I)$)	$R_1 = 0.0313$, $wR_2 = 0.0764^a$	$R_1 = 0.0423$, $wR_2 = 0.1148^b$	$R_1 = 0.0365$, $wR_2 = 0.0904^c$
Final R value (all data)	$R_1 = 0.0342$, $wR_2 = 0.0813^a$	$R_1 = 0.0529$, $wR_2 = 0.1294^b$	$R_1 = 0.0429$, $wR_2 = 0.1120^c$
$(\Delta/\rho)_{\text{max}}$ ($\text{e}^- \text{ \AA}^{-3}$)	0.385	0.805	0.754
$(\Delta/\rho)_{\text{min}}$ ($\text{e}^- \text{ \AA}^{-3}$)	-0.413	-0.430	-0.381

^a Calc. $w = 1/[\sigma^2(F_o^2) + (0.0267P)^2 + 1.2528P]$, where $P = (F_o^2 + 2F_c^2)/3$.

^b Calc. $w = 1/[\sigma^2(F_o^2) + (0.0589P)^2 + 3.0419P]$, where $P = (F_o^2 + 2F_c^2)/3$.

^c Calc. $w = 1/[\sigma^2(F_o^2) + (0.0410P)^2 + 0.6786P]$, where $P = (F_o^2 + 2F_c^2)/3$.

All hydrogen atoms were placed on calculated positions, except for the positions of the protons bonded to the oxygen atoms O(2) and O(3) of methanol in **3** which were taken from the Fourier map, and allowed to ride on their corresponding carbon atoms. The isotropic thermal parameters for the methyl protons were refined 1.5 times and for all other hydrogen atoms 1.2 times the U_{eq} value of the bonding atom. The hydroxo protons of the solvate molecules in **3** were located in the difference Fourier map and refined 1.5 times the U_{eq} value of the corresponding atom. The methyl protons were placed on calculated positions ($U_H = 1.5U_{eq}$ of the bonded atom) in staggered conformation with respect to the hydroxo groups. All other non-hydrogen atoms of the complexes were refined anisotropically.

2.9. Catechol 1,2-dioxygenase activity

The catechol cleaving activity of the iron(III) complexes containing 3,5-di-tert-butylcatechol (dbc) and pyrocatechol (cat) and the ligands bpia and bipa were performed on in situ prepared complexes. To 2 cm³ of a 5×10^{-4} mol dm⁻³ solution consisting of iron(III)perchlorate nonahydrate and the ligand were added 0.02 cm³ of a 5×10^{-2} mol dm⁻³ (1 equiv.) solution of the catechol and 0.04 cm³ of a 5×10^{-2} mol dm⁻³ (2 equiv.) solution of piperidine. Air saturated methanol was used as solvent. The disintegration of the iron(III)–catecholate complexes was monitored by UV–Vis spectroscopic measurements at ambient temperature (25°C). Kinetic analyses of the intradiol cleaving reactions were carried out by time dependent measurements of the lower energy catecholate–iron(III) charge-transfer band.

3. Results and discussion

The ligands bpia and bipa (Fig. 2) have been prepared following a modified literature method [24]. On addition of a solution of iron(III) salts to a solution of the ligand the compounds [Fe(bpia)Cl₂][FeCl₄] (**1**), [Fe(bipa)Cl₂](ClO₄) (**2**), and [Fe₂O(bpia)₂Cl₂](Cl₂·4MeOH) (**3**) have been obtained. The iron cores have a distorted octahedral coordination sphere in common. The ligands consist of pyridine and imidazole moieties so that N₄ donor sets are provided. The *cis* coordination sites, necessary for catalytic activity, are either occupied by two labile chloro ligands or by a chloro and a bridging oxo ligand. Crystallographic and experimental details are given in Table 1. Relevant distances and angles of the complexes are shown in Tables 2 to 4.

These mononuclear and binuclear motifs with N₄ donor sets of different ligands have been reported pre-

Table 2
Selected bond lengths (Å) and angles (°) for **1**

Bond lengths (Å)			
Fe(1)–Cl(1)	2.2939(10)	Fe(1)–Cl(2)	2.2442(10)
Fe(1)–N(1)	2.125(3)	Fe(1)–N(2)	2.271(3)
Fe(1)–N(3)	2.116(3)	Fe(1)–N(4)	2.104(3)
Bond angles (°)			
Cl(1)–Fe(1)–Cl(2)	99.59(4)	Cl(1)–Fe(1)–N(1)	90.62(9)
Cl(1)–Fe(1)–N(2)	92.61(8)	Cl(1)–Fe(1)–N(3)	90.09(8)
Cl(1)–Fe(1)–N(4)	170.20(8)	Cl(2)–Fe(1)–N(1)	102.55(8)
Cl(2)–Fe(1)–N(2)	167.77(8)	Cl(2)–Fe(1)–N(3)	104.73(8)
Cl(2)–Fe(1)–N(4)	90.21(8)	N(1)–Fe(1)–N(2)	76.24(11)
N(1)–Fe(1)–N(3)	152.20(11)	N(1)–Fe(1)–N(4)	86.97(11)
N(2)–Fe(1)–N(3)	75.96(11)	N(2)–Fe(1)–N(4)	77.59(10)
N(3)–Fe(1)–N(4)	87.65(11)		

Table 3
Selected bond lengths (Å) and angles (°) for **2**

Bond lengths (Å)			
Fe(1)–Cl(1)	2.2717(10)	Fe(1)–Cl(2)	2.2490(10)
Fe(1)–N(1)	2.136(3)	Fe(1)–N(2)	2.304(3)
Fe(1)–N(3)	2.077(3)	Fe(1)–N(5)	2.108(2)
Bond angles (°)			
Cl(1)–Fe(1)–Cl(2)	100.64(4)	Cl(1)–Fe(1)–N(1)	89.09(8)
Cl(1)–Fe(1)–N(2)	92.61(7)	Cl(1)–Fe(1)–N(3)	91.79(8)
Cl(1)–Fe(1)–N(5)	168.05(7)	Cl(2)–Fe(1)–N(1)	105.58(8)
Cl(2)–Fe(1)–N(2)	166.61(7)	Cl(2)–Fe(1)–N(3)	102.05(8)
Cl(2)–Fe(1)–N(5)	90.29(7)	N(1)–Fe(1)–N(2)	76.30(10)
N(1)–Fe(1)–N(3)	151.70(11)	N(1)–Fe(1)–N(5)	83.29(10)
N(2)–Fe(1)–N(3)	75.40(10)	N(2)–Fe(1)–N(5)	76.68(9)
N(3)–Fe(1)–N(5)	90.60(10)		

Table 4
Selected bond lengths (Å) and angles (°) for **3**

Bond lengths (Å)			
Fe(1)⋯Fe(1a)*	3.5756(8)		
Fe(1)–O(1)	1.7878(6)	Fe(1)–Cl(1)	2.2991(9)
Fe(1)–N(1)	2.156(2)	Fe(1)–N(2)	2.266(2)
Fe(1)–N(3)	2.154(2)	Fe(1)–N(4)	2.157(2)
Bond angles (°)			
Fe(1)–O(1)–Fe(1a)	180.0	O(1)–Fe(1)–Cl(1)	101.40(3)
O(1)–Fe(1)–N(1)	92.88(6)	O(1)–Fe(1)–N(2)	93.71(5)
O(1)–Fe(1)–N(3)	89.15(5)	O(1)–Fe(1)–N(4)	169.32(5)
Cl(1)–Fe(1)–N(1)	102.45(6)	Cl(1)–Fe(1)–N(2)	164.85(5)
Cl(1)–Fe(1)–N(3)	103.92(6)	Cl(1)–Fe(1)–N(4)	88.37(6)
N(1)–Fe(1)–N(2)	75.55(7)	N(1)–Fe(1)–N(3)	152.59(7)
N(1)–Fe(1)–N(4)	89.13(7)	N(2)–Fe(1)–N(3)	77.07(7)
N(2)–Fe(1)–N(4)	76.64(7)	N(3)–Fe(1)–N(4)	84.28(7)

* Symmetry transformation: 1–x, 1–y, 1–z.

viously [11,12]. Table 5 gives an overview of related complexes.

3.1. Crystal structures of [Fe(bpia)Cl₂][FeCl₄] (**1**) and [Fe(bipa)Cl₂](ClO₄) (**2**)

Compound **1** crystallizes with two complex cations [Fe(bpia)Cl₂]⁺ and two complex counter ions [FeCl₄][–]

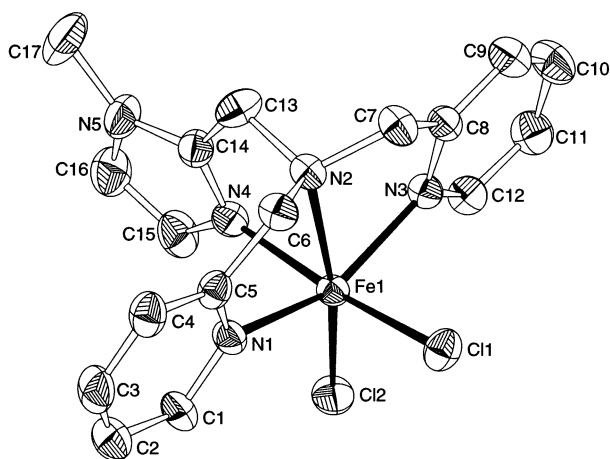


Fig. 3. ORTEP plot of $[\text{Fe}(\text{bpia})\text{Cl}_2]^+$; hydrogen atoms omitted for clarity.

per unit cell. The structure of **2** is closely related to that of **1**. The ligand bpia is replaced by the ligand bipa and a perchlorate ion acts as a counter ion. The unit cell of **2** contains four formula units. Figs. 3 and 4 show the cations of **1** and **2**. Both complexes exhibit a N_4Cl_2 coordination sphere. The N_4 donor sets are provided by the ligands bpia (**1**) and bipa (**2**). Due to the limiting bite of both ligands the coordination polyhedron is distorted octahedral. With respect to the nature of the N donor moieties the largest Fe–N bond length in these mononuclear complexes occurs between Fe(1) and N(2). In general, compared to the tertiary amine nitrogen the nitrogen atoms of the aromatic heterocycles bond more strongly to the iron center because the tertiary amine has a lower ability to act as a π -donor. In contrast to this the N donor atoms of the aromatic heterocycles exhibit shorter bond lengths with an average value of 2.115 Å for **1** and 2.107 Å for **2**, respec-

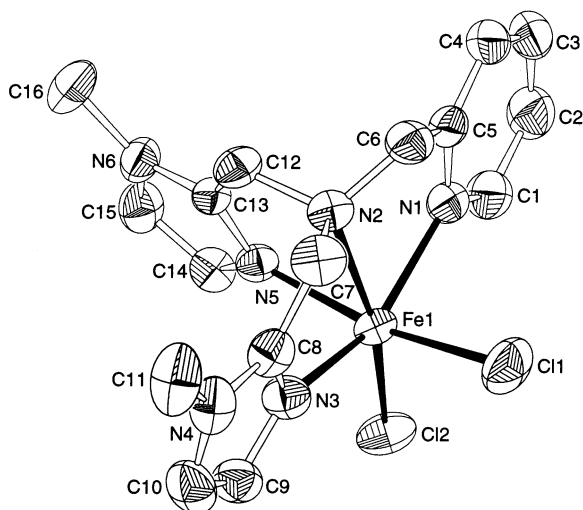


Fig. 4. ORTEP plot of $[\text{Fe}(\text{bipa})\text{Cl}_2]^+$; hydrogen atoms omitted for clarity.

Table 5
Comparison of selected bond lengths and spectroscopic data

	Fe...Fe (Å)	Fe–O (Å)	Fe–O (Å)	Fe–Cl (Å)	Fe– $\text{N}_{\text{trans oxo}}$ (Å)	λ_{max} (nm)	ϵ ($\text{cm}^2 \text{mol}^{-1}$)	$-J$ (cm^{-1})	$E_{1/2}$ (V)	Reference
$[\text{Fe}(\text{bpia})\text{Cl}_2][\text{FeCl}_4]$				2.294(1) 2.244(1)		362	3240		0.614	this work
$[\text{Fe}(\text{bipa})\text{Cl}_2][\text{ClO}_4]$				2.249(1) 2.272(1)		372	3025		0.330	this work
$[\text{Fe}(\text{tpa})\text{Cl}_2][\text{ClO}_4]$				2.224(2) 2.267(2)		382	3170			[11]
$[\text{Fe}_2\text{O}(\text{bpia})_2\text{Cl}_2] \cdot 4\text{MeOH}$	3.5756(8)	1.788(1)	180(0)	2.299(1)	2.157(2)	312, 367	4880, 3840	116	0.095	this work
$[\text{Fe}_2\text{O}(\text{tpa})_2\text{Cl}_2][\text{ClO}_4]_2$	3.581(2)	1.790(1)	179,98(0)	2.319(1)	2.263(6)	380	8300	109,7		[11]
$[\text{Fe}_2\text{O}(\text{ntb})_2\text{Cl}_2][\text{PF}_6]_2 \cdot 4\text{THF}$	3.610(1)	1.805(1)	180(0)	2.293(1)	2.249(5)	300, 401	4500, 3630	100	0.580	[12]

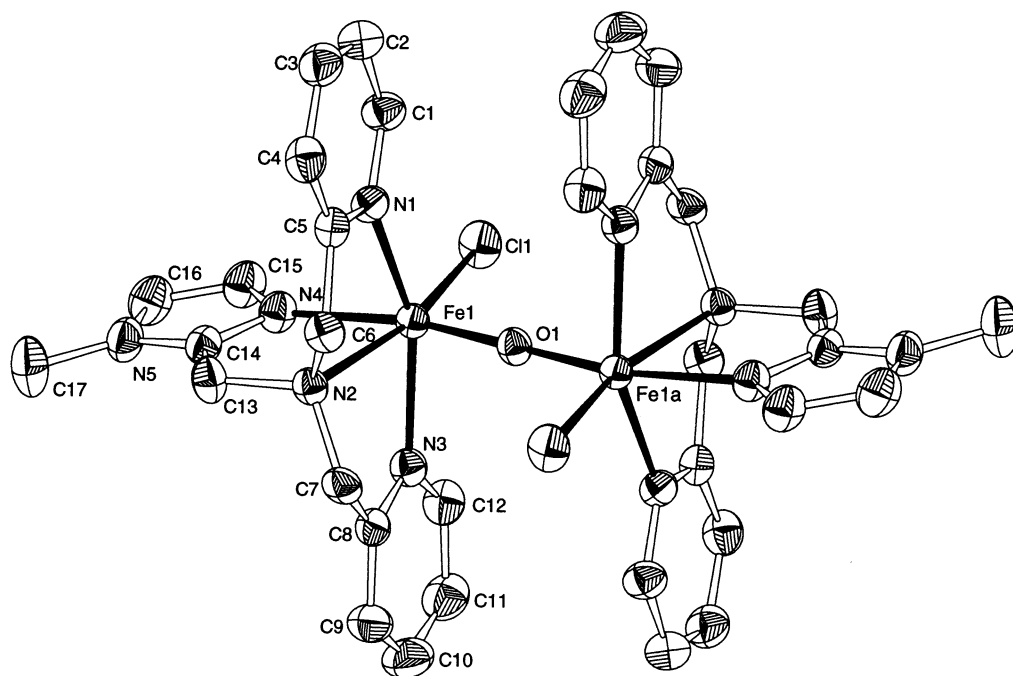


Fig. 5. ORTEP plot of $[\text{Fe}_2\text{O}(\text{bpia})_2\text{Cl}_2]^{2+}$; hydrogen atoms omitted for clarity.

tively. In compound **2** the *trans* effect becomes apparent in the extended bond length of one imidazole part (N(5)), whereas the same bond length in compound **1** shows an even shorter value than the others. In this case steric interactions between the large FeCl_4^- counter ions and the complex cation play a role. The chloro ligands have in both complexes approximately the same mean bond length. As in compound **2** the similar tpa (tris(2-pyridylmethyl)amine) complex exhibits a *trans* effect of the chloride ligands that results in a lengthened $\text{Fe}-\text{N}_{\text{pyridine}}$ bond [11]. In this case also a small counter ion (ClO_4^-) has been used. Due to the higher Lewis acidic character of the tpa-iron core the chloro bond lengths are shortened.

The octahedron is distorted towards the tertiary amino group. This is reflected in the low average value of the angles between the tertiary amine donor and the pyridine/imidazole moieties (76.6° for **1**; 76.1° for **2**). Consequently the angles between the two chloro ligands are expanded (99.6° for **1**; 100.6° for **2**).

3.2. Crystal structure of $[\text{Fe}_2\text{O}(\text{bpia})_2\text{Cl}_2]\text{Cl}_2 \cdot 4\text{MeOH}$ (**3**)

The unit cell of compound **3** consists of one complex cation $[\text{Fe}_2\text{O}(\text{bpia})_2\text{Cl}_2]^{2+}$, two chloride anions and four methanol solvate molecules. The cation is shown in Fig. 5. Both iron cores have a N_4OCl donor set forming a distorted octahedron. They are bridged by the oxygen atom O(1) which is located on the center of

inversion. Consequently the μ -oxo dimer has a linear $\text{Fe}-\text{O}-\text{Fe}$ structure (180°). The $\text{Fe}(1)-\text{O}(1)$ bond length is $1.788(1)$ Å resulting in an $\text{Fe}\cdots\text{Fe}$ separation of $3.5756(8)$ Å. The tetradentate ligand bpia consists of one methylimidazole and two pyridine moieties connected to a tertiary amine. The sixth coordination site is occupied by a terminally bonded chloride atom. The two pyridine nitrogen atoms (N_1, N_3) and the tertiary amino group are *cis* oriented while the imidazole (N_4) part binds *trans* to the bridging oxo ligand.

The same reasons as described for **1** and **2** cause the expanded bond length of the tertiary amine donor. This is reflected in the bond lengths of the coordinated

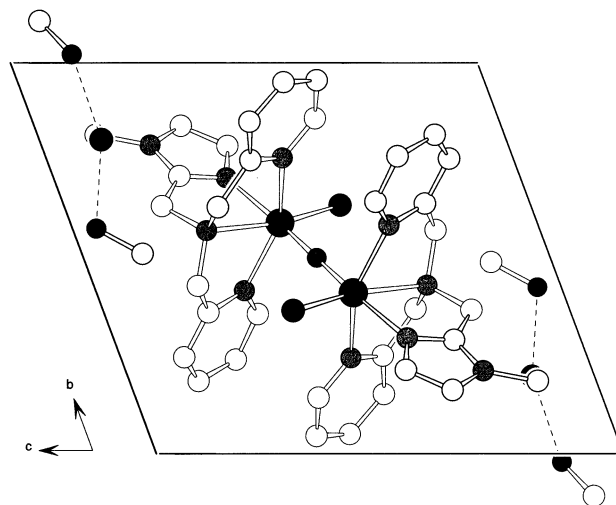


Fig. 6. Cell plot of compound **3**.

heterocycle atoms (2.156(2) Å for Fe(1)–N(1), 2.154(2) Å for Fe(1)–N(3) and 2.157(2) Å for Fe(1)–N(4)) exhibiting almost the same bond lengths. One exception is the bond length of the tertiary amine (2.266(2) Å for Fe(1)–N(2)). With respect to steric interactions between the imidazole moiety of the ligand and the counter ion no *trans* effect of the oxo bridge appears. The distortion of the octahedron occurs towards the tertiary amino group. The *cis* angles are decreased due to the limiting bite of the ligand (average value of 76.4°).

The distortion of the coordination polyhedron is caused partly by interactions between opposite ligands. In the similar ntb (tris(2-benzimidazolylmethyl)amine) complex steric effects result in a linear oxo bridge [12]. The cocrystallization with its mononuclear pendant leads in the case of the tpa compound to a complex of lower crystallographic symmetry. Thus, the angle Fe(1)–O(1)–Fe(1a) has a value of 179.98(0)° [11].

There are hydrogen bonds between two methanol solvate molecules and one chloride anion as shown in the cell plot (Fig. 6).

3.3. IR and electronic spectra

For further characterization the IR and electronic absorption spectra have been determined.

The UV–Vis spectroscopic properties of the complexes are listed in Table 5. For **1** and **2** absorption features ascribed to the charge transfer transitions from Cl[−] to Fe(III) are observed at 326 nm ($\epsilon = 3240 \text{ cm}^2 \text{ mol}^{-1}$), and 372 nm ($\epsilon = 3025 \text{ cm}^2 \text{ mol}^{-1}$), respectively. The UV–Vis spectrum of complex **3** exhibits a band at 367 nm ($\epsilon = 3840 \text{ cm}^2 \text{ mol}^{-1}$) and a shoulder at 312 nm ($\epsilon = 4880 \text{ cm}^2 \text{ mol}^{-1}$) which can be assigned to oxo Fe(III) and Cl[−] → Fe(III) charge transfer transitions. The bands below 250 nm are caused by π – π^* transitions of the ligand. The slight differences in wavelengths of the similar complexes (Table 5) can be correlated with the electron donor abilities of the tetradentate ligands. Thus, conclusions about the Lewis acidity of the iron cores can be drawn. A higher electrophilic character of the metal ion shifts the charge transfer transitions to higher wavelengths.

The IR spectra of the complexes show the typical aromatic and aliphatic bands. A strong band in the spectrum of **3** can be assigned to $\nu(\text{O–H, CH}_3\text{OH})$ at 3321 cm^{−1}. The coordination of the imidazole and pyridine moieties causes a shift of the aromatic C=N bands to higher wavenumbers.

3.4. Electrochemistry

The cyclovoltammograms of the two mononuclear complexes each exhibit a reduction and oxidation

wave that can be assigned to one-electron processes (Fe(III)/Fe(II)). The $E_{1/2}$ values are 0.614 V for **1** and 0.330 V for **2**. These potentials are quasi-reversible by definition [27]. The observed values reflect the order expected from the UV–Vis spectroscopic experiments. The spectrum of **3** shows a single irreversible reduction wave at −0.9 V and a coupled oxidation–reduction wave at 0.293 and −0.086 V. The resulting $E_{1/2}$ value is 0.095 V. The redox process is irreversible by definition. The irreversible wave at −0.9 V can be either assigned to a one-electron reduction process resulting in a mixed valence oxidation state or a cleavage of the μ -oxo bridge due to a one-electron reduction [28]. The first case corresponds to the redox couple Fe₂(III,III)/Fe₂(III,II), the second to Fe(III)/Fe(II).

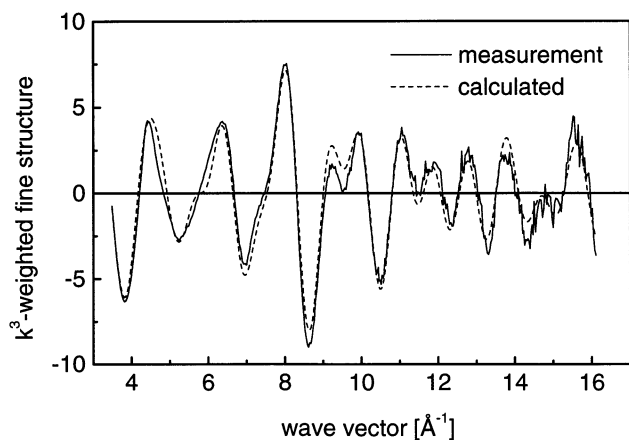
Species related to the complexes show similar electrochemical properties [12]. The dinuclear tpa complex described by Que and coworkers is an exception as compared to the analogous ntb and bpia complexes due to the cocrystallization with its mononuclear pendant [11].

3.5. Mössbauer spectroscopy and magnetic susceptibility

A pair of Lorentzians with identical amplitude and linewidth was used to fit the ⁵⁷Fe Mössbauer spectrum of **1**. The existence of octahedral high-spin iron(III) ions is confirmed by one distinct symmetrical quadrupole doublet exhibiting a δ_1 value of 0.50 mm s^{−1} and a ΔE_{Q1} value of 1.87 mm s^{−1}. The value δ_1 is in the normal range observed for high-spin iron(III) complexes (0.3 < δ < 0.6 mm s^{−1}) [29]. The quadrupole splitting reflecting the field gradient at the nucleus suggests an equivalent N₄OCl coordination sphere at both metal cores. The value of the quadrupole splitting indicates considerable distortions from octahedral symmetry.

The susceptibility shows a minimum at 45 K. μ_{eff} has a value of 0.45 μ_{B} at 4.5 K which rises with increasing temperature to 2.91 μ_{B} at 320 K indicating antiferromagnetic coupling between the iron centers. The exchange constant J was obtained by least-squares fit of the theoretical expression with $H = -2JS_1S_2$ to the experimental $\chi(T)$ data assuming a TIP of 400×10^{-6} emu/mol per Fe(III) ion and a fixed g -factor of 2.00, giving a value of $-J = 116 \text{ cm}^{-1}$.

For similar compounds with a linear bridging, oxo ligand values of 109.7 cm^{−1} (tpa) and 100 cm^{−1} (ntb) for $-J$ have been observed (Table 5) [11,12], in accordance with the overall range of $-J = 80$ – 120 cm^{-1} for both linear and slightly bent μ -oxo bridged diiron complexes [30,31].

Fig. 7. k^3 -weighted fine structures of 3.

3.6. Extended X-ray absorption fine structure (EXAFS) spectroscopy

Compound 3 is the one of the first dinuclear iron(III) compounds containing a 180° oxo bridge that is investigated by EXAFS spectroscopy [17]. Figs. 7 and 8 show the comparison of the k^3 -weighted fine structures and their corresponding Fourier transforms. The first peak in the Fourier transform at about 2 Å is broad, suggesting different metal ligand distances. The intense peak at 3.5 Å suggests that a Fe–Fe interaction and multiple scattering contributions arising from the 180° oxo bridge are involved. Peaks I, II, and III were isolated together to minimize any possible distortions from Fourier filtering and to take into account multiple scattering contributions. It is impossible to fit the three peaks with reasonable values applying single scattering calculations. In contrast to that a good fit was obtained by applying multiple scattering calculations assuming the presence of one Fe–O, one Fe–Cl, one Fe–N_{im}, three Fe–N and one Fe–Fe interaction. Bond lengths and structure of the complex indicated by EXAFS analysis agree in a perfect manner with those shown by

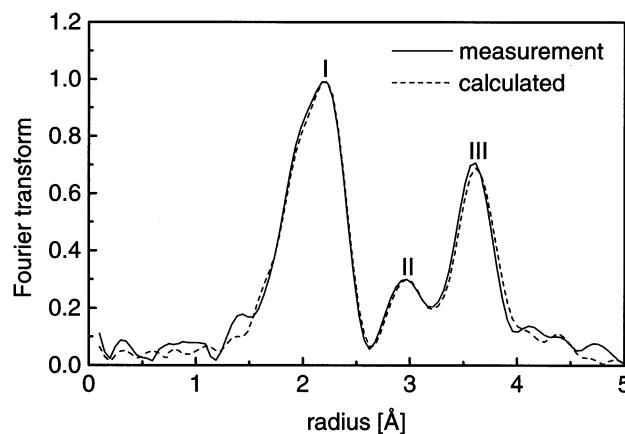


Fig. 8. Fourier transformations of 3.

the crystallographic analysis (Table 6), including a short Fe–O bond at 1.78 Å. The angle Fe(1)–N(4)–C(15) determined by crystallographic analysis is 137° . The multiple scattering refinement performed in this case gives an angle of 137° which agrees perfectly with the crystallographically determined angle (Fig. 9).

3.7. Catechol 1,2-dioxygenase activity

In the first step of the catechol dioxygenase reaction catecholate binds to the iron core. This is displayed in a color change of the solution from yellow to dark purple. In the UV–Vis spectra two bands appear in the range from 500 to 900 nm that can be assigned to charge transfer transitions from catecholate to iron. The transformation of the substrate by reaction with oxygen to a derivative of *cis,cis*-muconic acid (Fig. 10) was observed by the decrease of the lower energy charge transfer band with time. A band at 400 nm corresponding to the oxidation product 3,5-di-*tert*-butyl-*ortho*-quinone or *ortho*-quinone, respectively, does not appear in the spectra. Fig. 10 shows the progress of the reaction of the bpia complex with dbc and O₂. The inset displays the logarithm of the absorp-

Table 6
Curve-fitting results for Fe–K EXAFS of 3^a

Window width (Å)	N_{free}	N and scatterer	R (Å)	σ^2 (Å ²)	E_0 (eV)	Φ (°)	R -factor (%)
1.3–4.7	30	1, O	1.789(3)	0.004(1)	17.3(3)		27.6
		1, Cl	2.321(4)	0.001(1)			
		3, N	2.111(3)	0.005(1)			
		1, N(im)	2.361(7)	0.001(3)		137.3(1)	
		1, C(im)	3.016(7)	0.001(1)			
		1, C(im)	3.381(7)	0.001(1)			
		1, C(im)	4.232(7)	0.017(5)			
		1, N(im)	4.349(7)	0.017(5)			
		1, Fe	3.648(3)	0.003(0)			

^a N is the number of scatterers per metal, R is the metal-scatterer distance, σ^2 is a mean square deviation in R . The fit was performed over the $k = 2\text{--}16 \text{ \AA}^{-1}$ range.

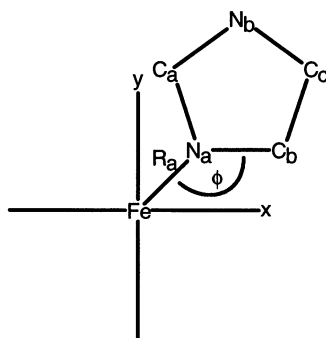


Fig. 9. Definition of the imidazole group.

tion versus time. The reactions show pseudo first order kinetics due to the excess of dioxygen dissolved in methanol ($2.12 \times 10^{-3} \text{ mol l}^{-1}$ at 25°C ; 25 times the amount of complex). Kinetic analyses have been carried out by calculation of the initial rates of the reaction rate constant. For the reaction of dbc the bpia complex exhibits a more than four times greater value compared to the bipa complex (Table 7). Using pyrocatechol (cat) as substrate the bpia complex shows an even higher activity (ca. six times) in contrast to the bipa complex [14].

From the position of the catechol \rightarrow iron(III) charge transfer band conclusions on the influence of the ligand properties can be drawn (Table 7). The UV–Vis absorption maxima shift to higher wavelengths, i.e. lower energy, with higher Lewis acidity of the iron core. The spectrum of the bipa–dbc complex exhibits a c.t. band at 842 nm, for the bpia–dbc complex the corresponding band is found at 865 nm. Therefore, the coordination of the ligand bpia leads to an iron(III) complex with a higher Lewis acidity. The higher electron accepting ability favors the formation of the second step in the reaction mechanism – a semiquinone species [8,9,13,32]. Similar conclusions can be drawn from the experiments

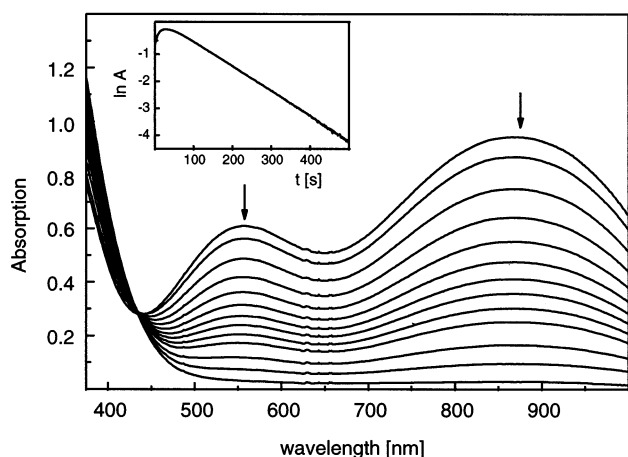


Fig. 10. Progress of the reaction of $[\text{Fe}(\text{bpia})(\text{dbc})]^+$ with O_2 (measurement interval: 15 s). Inset: Plot of $\ln(\text{Abs})$ vs. t for the $[\text{Fe}(\text{bpia})(\text{dbc})]^+$ reaction at 25°C .

Table 7

Kinetic and spectroscopic properties of the in situ prepared complexes

	Reaction rate constant ($\text{M}^{-1} \text{s}^{-1}$)	Lower energy c.t. band (nm)
$[\text{Fe}(\text{bpia})(\text{dbc})]^+$	4.3	865
$[\text{Fe}(\text{bipa})(\text{dbc})]^+$	0.98	842
$[\text{Fe}(\text{bpia})(\text{cat})]^+$	0.089	729
$[\text{Fe}(\text{bipa})(\text{cat})]^+$	0.015	718

with pyrocatechol. The reaction rate constants for the cat complexes are significantly smaller (about 50 times) which results from the lower electron donating character of cat. Therefore, the energies of the LMCT bands observed for the complexes with cat are higher (729 nm for bpia; 718 nm for bipa) than those observed for dbc. This is due to the electron donating character of the tert-butyl groups in dbc.

In former investigations by Que et al. the degradation of the isolated compound $[\text{Fe}(\text{tpa})(\text{dbc})]\text{BPh}_4$ has been determined [9]. This complex exhibits an even higher reactivity ($k = 10 \text{ M}^{-1} \text{s}^{-1}$) than the bpia compound as expected from the spectroscopic data of the chloro complexes (Table 5).

In summary, large reaction rate constants result from a high electrophilic, i.e. high Lewis acidic, character of the iron(III) complex caused by the ligand. The reaction rate constants are additionally influenced by a high nucleophilic character of the substrate caused by the substituents of the catechol.

4. Conclusions

A series of complexes as functional and structural models for catechol 1,2-dioxygenases have been prepared. In all three compounds the iron centers are distorted octahedrally coordinated by the tetradentate tripodal ligands bpia and bipa that provide N_4 donor sets and either two chloro ligands (**1**, **2**) or a chloro and a bridging oxo ligand resulting in a dinuclear species (**3**). The structures of these complexes could be obtained by X-ray crystallography.

We investigated the effects of these ligand sets with imidazole moieties on the reactivity of catechol 1,2-dioxygenase. For the in situ prepared complexes the catechol cleaving activity of the bpia complexes is significantly higher than for the bipa complexes. 3,5-Di-tert-butylcatechol exhibits a higher reactivity than pyrocatechol. The differences in reactivity are reflected in the UV–Vis spectra of the catecholato complexes. The position of the dbc/cat \rightarrow Fe(III) c.t. band is influenced by the ligands and by the substituents of the catechols. Therefore, the bpia–dbc complex exhibits the highest Lewis acidity of the iron core, the highest

electron donating character of the catechol, and consequently the lowest energy of the LMCT band among the examined complexes. The conclusions support the substrate activation mechanism by Que et al. [8,9,13,32].

In spite of some minor structural differences these three compounds fit perfectly into the context of similar complexes (Table 5) [11,12]. Within the mononuclear species a trend in Lewis acidity of the iron core becomes apparent. This is reflected in the position of c.t. bands and in the catechol 1,2-dioxygenase reactivity. Similar relationships for the UV–Vis spectra of the three dinuclear species were found; the antiferromagnetic coupling correlates with the separation of the iron cores.

The EXAFS work contributes to the general problem of linear monoatomic linear bridges that may occur in synthetic and biological assemblies. From our multiple scattering calculations accurate metric determinations of distances and angles were obtained.

The catechol 1,2-dioxygenase reactivity of iron(III) complexes of further ligand systems with new substrates is under investigation.

5. Supplementary material

Further details of the crystal structure investigation, atomic coordinates, thermal parameters, complete bond distances and angles can be obtained from the Cambridge Crystallographic Data Centre, 12 Union Road, Cambridge CB2 1EZ, UK, on quoting the full journal citation.

Acknowledgements

Financial support from the Henkel KGaA, the Deutsche Forschungsgemeinschaft, the Volkswagen Foundation, the Bundesministerium für Bildung und Forschung and the Fonds der Chemischen Industrie is gratefully acknowledged. We thank Professor W. Haase and K. Falk (Technische Universität Darmstadt) for magnetic susceptibility measurements. M.P. thanks the Ministerium für Schule und Weiterbildung, Wissenschaft und Forschung des Landes Nordrhein-Westfalen for a Graduiertenstipendium.

References

- [1] P.L. Roach, I.J. Clifton, C.M.H. Hensgens, N. Shibata, C.J. Schofield, J. Hajdu, J.E. Baldwin, *Nature* 387 (1997) 827.
- [2] W. Minor, J. Steczko, B. Stec, Z. Otwinowski, J.T. Bolin, R. Walter, B. Axelrod, *Biochemistry* 35 (1996) 10687.
- [3] (a) D.H. Ohlendorf, A.M. Orville, J.D. Lipscomb, *J. Mol. Biol.* 244 (1994) 586. (b) T. Senda, K. Sygiyama, H. Narita, T. Yamamoto, K. Kimbara, M. Fukuda, M. Sato, K. Yano, Y. Mitsui, *J. Mol. Biol.* 255 (1996) 735. (c) S.J. Lange, L. Que Jr., *Curr. Opin. Chem. Biol.* 2 (1998) 159.
- [4] R.B. Lauffer, R.H. Heistand II, L. Que Jr., *Inorg. Chem.* 22 (1983) 50.
- [5] W.O. Koch, H.-J. Krüger, *Angew. Chem.* 107 (1995) 2928; *Angew. Chem. Int. Ed. Engl.* 34 (1995) 2671.
- [6] M. Ito, L. Que Jr, *Angew. Chem.* 109 (1997) 1401; *Angew. Chem. Int. Ed. Engl.* 36 (1997) 1342.
- [7] Y. Nishida, H. Shimo, S. Kida, *J. Chem. Soc., Chem. Commun.* (1984) 1611.
- [8] D.D. Cox, L. Que Jr, *J. Am. Chem. Soc.* 110 (1988) 8085.
- [9] H.G. Jang, D.D. Cox, L. Que Jr, *J. Am. Chem. Soc.* 113 (1991) 9200.
- [10] R. Viswanathan, M. Palaniandavar, T. Balasubramanian, T.P. Muthiah, *Inorg. Chem.* 37 (1998) 2943.
- [11] T. Kojima, R.A. Leising, S. Yan, L. Que Jr, *J. Am. Chem. Soc.* 115 (1993) 11328.
- [12] R.M. Buchanan, R.J. O'Brien, J.F. Richardson, J.-M. Latour, *Inorg. Chim. Acta* 214 (1993) 33.
- [13] L. Que Jr, R.C. Kolanczyk, L.S. White, *J. Am. Chem. Soc.* 109 (1987) 5373.
- [14] M. Duda, M. Pascaly, B. Krebs, *J. Chem. Soc., Chem. Commun.* (1997) 835.
- [15] R. Viswanathan, M. Palaniandavar, *J. Chem. Soc., Dalton Trans.* (1995) 1259.
- [16] B.-K. Teo, *J. Am. Chem. Soc.* 103 (1981) 3990.
- [17] M.S. Co, W.A. Hendrickson, K.O. Hodgson, S. Doniach, *J. Am. Chem. Soc.* 105 (1983) 1144.
- [18] (a) L. Merz, W. Haase, *J. Chem. Soc., Dalton Trans.* (1980) 875. (b) S. Gehring, P. Fleischhauer, H. Paulus, W. Haase, *Inorg. Chem.* 32 (1993) 54.
- [19] O. Kahn, *Molecular Magnetism*, VCH, NY, 1993.
- [20] S. Priggemeyer, P. Eggers-Borkenstein, F. Ahlers, G. Henkel, M. Körner, H. Witzel, H.-F. Nolting, C. Hermes, B. Krebs, *Inorg. Chem.* 34 (1995) 1445.
- [21] F. Zippel, F. Ahlers, R. Werner, W. Haase, H.-F. Nolting, B. Krebs, *Inorg. Chem.* 35 (1996) 3409.
- [22] N. Binsted, J.W. Campbell, S.J. Gurman, P.C. Stephenson, EXCURV92 program, SERC Daresbury Laboratory, UK, 1992.
- [23] N. Binsted, R.W. Strange, S.S. Hasnain, *Biochemistry* 31 (1992) 12117.
- [24] N. Wei, N.N. Murthy, Z. Tyeklár, K.D. Karlin, *Inorg. Chem.* 33 (1994) 1177.
- [25] C.B. Reese, Z. Pei-Zhou, *J. Chem. Soc., Perkin Trans.* (1993) 2291.
- [26] (a) G.M. Sheldrick, SHELXTL PLUS, Siemens Analytical X-Ray Instruments, Madison, WI, 1990. (b) G.M. Sheldrick, SHELXL 93, Program for Crystal Structure Determination, University of Göttingen, 1993.
- [27] A.J. Bard, L.R. Faulkner, *Electrochemical Methods*, Wiley, New York, 1980.
- [28] J.R. Hartman, R.L. Rardin, P. Chaudhuri, K. Pohl, K. Wiegardt, B. Nuber, J. Weiss, G.C. Papaefthymiou, R.B. Frankel, S.J. Lippard, *J. Am. Chem. Soc.* 109 (1987) 7387.
- [29] P. Gülich, R. Link, A.X. Trautwein, *Mössbauer Spectroscopy and Transition Metal Chemistry*, Springer, NY, 1978.
- [30] D.M. Kurtz Jr., *Chem. Rev.* 90 (1990) 585.
- [31] R. Hotzelmann, K. Wiegardt, U. Flörke, H.-J. Haupt, D.C. Weatherburn, J. Bonvoisin, G. Blondin, J.-J. Girerd, *J. Am. Chem. Soc.* 114 (1992) 1681.
- [32] R.Y.N. Ho, L. Que Jr., *Chem. Rev.* 96 (1996) 2607.